1

2

3

4

5 **Smectite formation in the presence of sulfuric acid: Implications for**

6 **acidic smectite formation on early Mars**

7

8

9

10

11 T.S. Peretyazhko[1*], P.B. Niles[2], B. Sutter[1], R. V. Morris[2], D. G. Agresti[3], L. Le[1], D.W. Ming[2]

12
13
14
15
16
17
18 [1] Jacobs, NASA Johnson Space Center, Houston, TX 77058
19
20 [2] NASA Johnson Space Center, Houston, TX 77058
21
21 [3] University of Alabama at Birmingham, Birmingham, AL 35294

22
23
24
25
26
27 Corresponding author: T. S. Peretyazhko, Jacobs, NASA Johnson Space Center,
28 Houston, TX 77058 (tanya.peretyazhko@nasa.gov)
29

30

31

32

33 In preparation for

Abstract

The excess of orbital detection of smectite deposits compared to carbonate deposits on the martian surface presents an enigma because smectite and carbonate formations are both favored alteration products of basalt under neutral to alkaline conditions. We propose that Mars experienced acidic events caused by sulfuric acid (H_2SO_4) that permitted phyllosilicate, but inhibited carbonate, formation. To experimentally verify this hypothesis, we report the first synthesis of smectite from Mars-analogue glass-rich basalt simulant (66 wt% glass, 32 wt% olivine, 2 wt% chromite) in the presence of H_2SO_4 under hydrothermal conditions (~200 °C). Smectites were analyzed by X-ray diffraction, Mössbauer spectroscopy, visible and near-infrared reflectance spectroscopy and electron microprobe to characterize mineralogy and chemical composition. Solution chemistry was determined by Inductively Coupled Plasma Mass Spectrometry. Basalt simulant suspensions in 11-42 mM H_2SO_4 were acidic with pH ≤ 2 at the beginning of incubation and varied from acidic (pH 1.8) to mildly alkaline (pH 8.4) at the end of incubation. Alteration of glass phase during reaction of the basalt simulant with H_2SO_4 led to formation of the dioctahedral smectite at final pH ~3 and trioctahedral smectite saponite at final pH ~4 and higher. Anhydrite and hematite formed in the final pH range from 1.8 to 8.4 while natroalunite was detected at pH 1.8. Hematite was precipitated as a result of oxidative dissolution of olivine present in Adirondack basalt simulant. Formation of secondary phases, including smectite, resulted in release of variable amounts of Si, Mg, Na and Ca while solubilization of Al and Fe was low. Comparison of mineralogical and solution chemistry data indicated that the type of smectite (i.e., dioctahedral vs trioctahedral) was likely controlled by Mg leaching from altering basalt and substantial Mg loss created favorable conditions for formation of dioctahedral smectite. We present a model for global-scale smectite formation on Mars via acid-sulfate conditions created by the volcanic outgassing of SO_2 in the Noachian and early Hesperian.

1. INTRODUCTION

60

61   Two global eras have been proposed to explain the observed mineralogy on Mars

62 (Bibring et al., 2006). Abundant phyllosilicates dominated by the smectite group (nontronite,

63 montmorillonite and saponite) were formed in the first era under water-rich neutral to alkaline

64 conditions during the Noachian. Formation of sulfate-bearing phases occurred in the second era

65 under acidic conditions likely caused by sulfuric acid during the Hesperian (Poulet et al., 2005;

66 Bibring et al., 2006; Murchie et al., 2009; Bishop et al., 2013). However, such simplified pH-

67 based division of aqueous history conflicts with some mineralogical observations. Large

68 carbonate deposits together with phyllosilicates would be a characteristic of a Noachian Mars

69 dominated by abundant liquid water, neutral/alkaline pH conditions, and a CO_2-rich atmosphere

70 (Fairén et al., 2004), but mineralogical observations have detected only isolated carbonate

71 deposits (Ehlmann et al., 2008; Milliken et al., 2009; Morris et al., 2010; Wray et al., 2016). The

72 absence of widespread carbonate deposits could result from carbonate deposition on early Mars

73 followed by its decomposition in acidic environments during Hesperian epoch (Fairén et al.,

74 2004; Bibring et al., 2006; Chevrier et al., 2007). Alternatively, abundant carbonates may never

75 have formed on early Mars because of short-term stability of liquid water and/or lack of dense

76 CO_2 atmosphere during Noachian epoch (Bibring et al., 2006; Chevrier et al., 2007; Niles et al.,

77 2013; Edwards and Ehlmann, 2015; Zolotov and Mironenko, 2016). Acidic events could also

78 explain the apparent lack of abundant carbonate/phyllosilicate associations, because carbonate

79 minerals do not form at acidic pH<6 conditions (Fairén et al., 2004; Fairén, 2013; Peretyazhko et

80 al., 2016; Zolotov and Mironenko, 2016). The carbonate/smectite mineralogical observation

81 might indicate that early Mars was not exclusively neutral-to-alkaline in pH but experienced

82　　local and perhaps widespread acidic events. As a result, smectite formation on Mars could occur

83　　not only under commonly expected neutral/alkaline conditions but also in acidic environments.

84　　　　　In terrestrial environments smectites formed under acidic conditions have been reported

85　　in acidic saline lakes, seafloor hydrothermal vents and fumarolic areas (Haymon and Kastner,

86　　1986; Story et al., 2010; Hynek et al., 2013). Limited laboratory observations have revealed

87　　smectite formation through hydrothermal basalt alteration in acidic pH 3-6 environments (Berger

88　　et al., 1987; Ghiara et al., 1993; Abdelouas et al., 1997; Dehouck et al., 2014). We have

89　　demonstated formation of saponite through alteration of Mars-analogue glass-rich basalt

90　　simulant in hydrothermal oxic and anoxic systems buffered by acetic acid (200 °C, pH_{RT} ~4 pH

91　　measured at room temperature, (Peretyazhko et al., 2016)).

92　　　　　The source of acidity on early Mars remains a subject for discussion. Two major acidity

93　　sources have been proposed for early Mars: (1) Fe(II) oxidative hydrolysis (Tosca et al., 2008;

94　　Hurowitz et al., 2010), and (2) volcanic release of sulfur dioxide, SO_2 (Zolotov and Mironenko,

95　　2007; Berger et al., 2009; Gaillard and Scaillet, 2009; Righter et al., 2009; Gaillard et al., 2013;

96　　Zolotov and Mironenko, 2016). We have previously hypothesized that sulfuric acid (H_2SO_4)

97　　produced by volcanic SO_2 degassing on early Mars was the major source of acidity for the

98　　alteration of basaltic materials and subsequent formation of smectite (Peretyazhko et al., 2016).

99　　Our hypothesis was supported by modeling and mineralogical observations. For instance, recent

100　　detection of smectite minerals co-existing with sulfates might indicate that basalt weathering and

101　　smectite formation occurred under acidic conditions caused by sulfuric acid (Farrand et al., 2009;

102　　Wray et al., 2011; Cavanagh et al., 2015; Flahaut et al., 2015; Rampe et al., 2017).

103　　Thermodynamic modeling of basalt interaction with H_2SO_4-rich solutions revealed formation of

104　　Al-rich phyllosilicates (kaolinite, montmorillonite) under mildly acidic conditions followed by

105　　Mg/Fe smectites at higher pH (Zolotov and Mironenko, 2007; Zolotov and Mironenko, 2016)

106 and modelling of Mars-like aqueous systems predicted coexistence of smectite and sulfate

107 minerals under mildly acidic pH 4-6 conditions (Fairén, 2013).

108   Formation of smectite through basalt alteration under Mars-relevant acid sulfate

109 conditions has not been experimentally studied and the effect of pH and the nature of forming

110 phyllosilicate minerals remains unknown. The objective of this work was to investigate

111 formation of smectite through hydrothermal alteration of Mars-analogue basalt in the presence of

112 sulfuric acid of variable concentrations, to assess acidity sources and to determine the extent to

113 which H_2SO_4 is the source of acidity on early Mars.

114

115   **2.   MATERIALS AND METHODS**

116

117 **2.1.   Synthesis and characterization of Adirondack basalt simulant**

118   Synthetic basalt simulant of composition similar to that for Adirondack class rocks

119 analyzed by the Mars Exploration Rover *Spirit* at Gusev Crater (McSween et al., 2006) was used

120 in smectite formation studies (hereafter, denoted as Adirondack basalt simulant). The detailed

121 synthesis procedure of the Adirondack basalt simulant is reported by Peretyazhko et al., (2016).

122 Briefly, a powdered mixture of reagent-grade oxides and carbonates was melted at 1400 °C in an

123 Au-Pt alloy crucible for 3d under the oxygen fugacity IW+1 (IW = iron-wüstite buffer) and

124 quenched in water. The glassy product was then crushed, ground and sieved to <53 μm particle

125 diameter for characterization and smectite formation experiments. X-ray diffraction analysis

126 revealed that Adirondack simulant contained 66 wt% X-ray amorphous glass, 32 wt% olivine

127 and 2 wt% chromite quench crystals within the glass matrix (Peretyazhko et al., 2016).

128 Composition of the glass phase, olivine and chromite are summarized in Table EA-1.

129

2.2. Hydrothermal smectite formation experiments and characterization

Adirondack basalt simulant suspensions of 17 g/l (water to rock ratio = 60) were prepared by mixing 250 mg simulant with 15 ml of solutions having variable H_2SO_4 concentrations (11.0 ± 0.1 mM, 13.6 ± 0.1 mM, 16.3 ± 0.1 mM, 21.9 ± 0.1 mM, 30.6 ± 0.3 mM and 42.5 ± 0.2 mM). Initial sulfuric acid concentrations were measured as total sulfate by ion chromatography as described below. Duplicate samples were placed in batch reactors (Teflon lined 23 ml Parr acid digestion vessel) and incubated in an oven at 200 °C for 14d. The temperature of 200 °C was chosen because hydrothermal conditions are favorable for smectite formation promoting breaking of chemical bonds and rapid basalt alteration (Berger et al., 2014). However, smectite formation through alteration of basalts has been shown to occur at lower temperatures (Seyfried et al., 1978; McMurtry and Yeh, 1981; Kloprogge et al., 1999; Hynek et al., 2013). Sample preparation and hydrothermal incubation were performed under ambient atmosphere (oxidizing conditions). Our previous study (Peretyazhko et al., 2016) demonstrated that smectite formed through alteration of Adirondack basalt simulant under oxidizing and reducing acidic hydrothermal conditions and that oxidizing conditions only affected Fe oxidation state in smectite.

Suspension pH was measured immediately after mixing Adirondack basalt simulant with H_2SO_4 (pH_{0d}) and after opening the reactors at the end of 14d incubation (pH_{14d}) with AccupHast pH electrode using Orion Star A329 meter. Both measurements were performed at room temperature (RT) of ~25 ºC. After pH measurement, solution was collected in a syringe and passed through a 0.2 μm syringe filter (PVDF, Fisherbrand). An aliquot of each filtered solution was acidified with ultra-pure HNO_3 (Fisher) for dissolved Ca, Mg, Na, Si, Al and Fe analysis by Inductively Coupled Plasma Mass Spectrometry (ICP-MS, Element XR Thermo Scientific) with argon as the carrier gas. The remaining solution was analyzed for sulfate by ion chromatography

154 using Dionex ICS-2000 equipped with Dionex IonPac AS18 column (4 x 250 mm), Dionex EGC

155 III KOH eluent and a suppressed conductivity detector Dionex AERS 500 4 mm with a 20 μm

156 injection volume.

157   Separated solids were dried in an oven at 40 °C for ~1h prior to analysis. X-ray

158 diffraction (XRD) patterns were recorded using a Panalytical X'Pert Pro with Co Kα radiation.

159 Samples were analyzed at 45 kV/40 mA with a 0.02° 2θ step for 1 min. Programmable divergent

160 and antiscatter slits were set to 1/4° with manual 1/2° antiscatter slit. The instrument was

161 operated under ambient conditions and calibrated with novaculite (quartz) standard (Gemdugout,

162 State College, PA). Standard powder mounts and low background silicon holders were used for

163 analyses of bulk samples and clay size fractions, respectively. Clay size fractions were separated

164 by ultrasonic dispersion (Kachanoski et al., 1988). Smectite-containing suspensions were

165 ultrasonically treated with a probe-type sonicator (Soniprep 150) for 10s. The suspension was

166 then allowed to sediment by gravity for ~1hr and supernatant containing the clay size fraction

167 was collected. The procedure was repeated until supernatant solutions became clear and the

168 collected clay fraction was separated by centrifugation. The clay fraction slurry was spread over

169 the low background holder with a pipette and dried at RT prior to analysis. Clay fractions were

170 treated with glycerol and KCl in order to confirm formation of smectite (Whittig and Allardice,

171 1986).

172   Visible and near-infrared reflectance (VNIR) spectra (0.35-2.5 μm) were measured with

173 an Analytical Spectral Devices FieldSpec3 fiber-optic based spectrometer with a reflectance

174 probe attachment (internal light source). Spectra were collected in absolute reflectance mode

175 using a Spectralon standard. Continuum removed spectra were obtained using ENVI software

176 (ENvironment for Visualizing Images, Harris Geospatial Solutions).

177   Mössbauer analyses were performed at RT under ambient conditions using MIMOS-II

178   instruments that are the laboratory equivalent of the instruments onboard the Mars Exploration

179   Rovers [SPESI, Inc., (Klingelhoefer et al., 2003)]. Velocity calibration was carried out with the

180   program MERView (Agresti et al., 2007) using the MIMOS-II differential signal and the

181   spectrum for metallic Fe foil acquired at RT. Mössbauer parameters [center shift (CS) with

182   respect to metallic Fe foil at RT, quadrupole splitting (QS), magnetic hyperfine field strength

183   (B_{hf}), and subspectral areas (A)] were obtained with a least-squares fitting procedure using

184   MERFit (Agresti and Gerakines, 2009). Reported values for A were converted to % Fe using the

185   f-factor ratio, $f_{Fe(III)}/f_{Fe(II)} = 1.21$ (Morris et al., 1995). Uncertainty for CS, QS, and full width at

186   half maximum (FWHM) was $\pm\ 0.02$ mm/s and uncertainty for A was $\pm\ 2\%$ absolute. The

187   following constraints were used in the least squares fitting procedure. (1) For each doublet, the

188   component peaks were constrained to have equal widths and areas. (2) Because of the low

189   observed intensity of hematite sextets, values for CS and QS were fixed to literature values

190   (e.g.,(Morris et al., 1985)), peak areas were constrained to 3 : x : 1 : 1 : x : 3, where x is variable

191   and FWHM decreased symmetrically toward zero velocity with skewed Lorentzian lineshapes.

192   Four representative samples were analyzed by Mössbauer spectroscopy covering the whole range

193   of the final pH_{14d} values.

194   Electron microprobe analyses of polished sections of smectite-containing Adirondack

195   basalt simulant were analyzed for elemental composition using a CAMECA SX-100 electron

196   microprobe (Figure EA-1). Backscattered electron imaging and analyses were collected at an

197   accelerating voltage of 15 kV and probe current of 20 nA with a spot size of 1 μm. Element

198   concentrations were calibrated using University of Tokyo Oxides standards. All measurements

199   were made under 20s peak counting and 10s background counting. Because of high water

200   content in smectite, total elemental content was lower than 100% in all analyzed samples. Data

201 with totals ≥74 wt% were used for smectite formula calculation. Residual sulfur and

202 phosphorous were considered as impurities and subtracted from the totals in formula

203 calculations. All Si atoms were assigned to tetrahedral sites and the remaining tetrahedral sites

204 were filled with Al (Al = 8-Si). The remaining Al atoms, Mg, Fe and minor Ti, Ni, Cr and Mn

205 were assigned to the octahedral sites, while Na, Ca and K were assigned to interlayer sites (Bain

206 and Smith, 1987).

207

2.3. Calculations of sulfur degassing on Mars

209   Crust production model and the amount of sulfur degassing from magma were used to

210 determine the release of SO_2 during Noachian/Early Hesperian epoch on Mars and then to obtain

211 the total amount of acidity (total amount of protons, H^+) produced from the oxidation of SO_2 to

212 H_2SO_4.

213   First, a crust production model described by Hirschmann and Withers (2008) was used to

214 calculate crust accumulation from early Noachian (~4.5 Ga) to late Amazonian (0 Ga). The

215 model is based on assumptions that crust formation is proportional to the heat flow and that total

216 crust production during 4.5 Ga is $654 \cdot 10^6$ km^3 as estimated by (Greeley and Schneid, 1991). The

217 model is described by the equation:

218
$$\frac{dV}{dt} = ae^{-ct} + be^{-dt} \qquad\qquad (1)$$

219 where variables are V (crust production) and t (time) and constants are a = $9.277 \cdot 10^5$ km^3, b =

220 $2.385 \cdot 10^5$ km^3, c = $6 \cdot 10^{-3}$ Ma^{-1}, d = $3.98 \cdot 10^{-4}$ Ma^{-1} (Hirschmann and Withers, 2008). The

221 calculated total crust production is shown in Figure EA-2. The amount of sulfur released from

222 magma was then calculated as

223   Total S= $S_{magma}\, \rho\, V$ (2)

224 where ρ is an average basalt density of 2800 kg/m^3 and S_{magma} is the amount of sulfur degassed

225 from magma of 2400 mg/kg (Righter et al., 2009).

226

3. RESULTS

228

3.1. pH before and after incubation

230   Different initial H_2SO_4 concentrations led to variable degrees of basalt neutralization

231 after 14d incubation. The average initial pH for all experiments was acidic ($pH_{0d} \leq 2$), and the

232 final pH_{14d} varied over a wide range including acidic (pH_{14d} 1.8 and 2.2), moderately acidic

233 (pH_{14d} 3.1 and 3.7), neutral (pH_{14d} 7.2) and slightly alkaline (pH_{14d} 8.4) (Figure 1).

3.2. Mineralogical characterization

3.2.1. X-ray diffraction

236   Powder XRD analyses of reaction products showed increasing phyllosilicate formation at

237 $pH_{14d} \geq 3$ on the basis of increasing intensity of the 001 diffraction peak at ~15 Å while no

238 phyllosilicate formation occurred at pH_{14d} 1.8 and 2.2 (Figure 2a, Table 1). After separation of

239 the clay size fraction, the phyllosilicate was identified as smectite based on expansion of the 001

240 peak to 17.4-18 Å after glycerol treatment, its collapse to 12.8 Å at room temperature upon KCl

241 addition, and its additional collapse to 10.1 Å after heating at 550 °C (Figure EA-3). The

242 positions of 02*l* and 060 d-spacings allowed distinguishing dioctahedral from trioctahedral

243 smectite (Moore and Reynolds, 1997; Vaniman et al., 2014). The 02*l* and 060 d-spacings

244 revealed that trioctahedral smectite formed at pH_{14d} 3.7, 7.2 and 8.4 and the peak positions

245 (Figure 2b, Table 2) were within the range reported for saponite (02*l*: 4.52-4.64 Å and 060: 1.53-

246 1.56 Å (Treiman et al., 2014; Chemtob et al., 2015; Peretyazhko et al., 2016)). The 02*l* and 060

247 d-spacings at 4.48 Å and 1.50 Å, respectively, indicated formation of dioctahedral smectite at

248   pH_{14d} 3.1 (Figure 2b, Table 2). The peak positions were in agreement with d-spacing reported for

249   montmorillonite (02*l*: 4.47 Å and 060: 1.492-1.504 Å, (Moore and Reynolds, 1997; Vaniman et

250   al., 2014)). However, formation of montmorillonite could not be confirmed with VNIR and

251   electron microprobe analyses (sections 3.2.3 and 3.2.4) and therefore phyllosilicate formed in the

252   pH_{14d} 3.1 sample is referred as dioctahedral smectite. Formation of smectite in all samples was

253   accompanied by decrease in intensity of the broad basaltic glass peak between 20° and 40° 2θ

254   with respect to the unaltered material (Figure 2a) suggesting glass as the smectite progenitor.

255   Anhydrite ($CaSO_4$) was found to precipitate at all values of pH_{14d} and natroalunite

256   ($NaAl_3(SO_4)_2(OH)_6$) was detected only at pH_{14d} 1.8 (Figure 2a, Table 1). A weak diffraction

257   peak of hematite (α-Fe_2O_3) was observed in the pH_{14d} 1.8 sample (Figure 2a, Table 1), and the

258   presence of hematite was confirmed by Mössbauer spectroscopy (Section 3.2.2). Hematite was

259   not detected in any other samples by XRD, but Mössbauer analysis showed that hematite was

260   present in the pH_{14d} range from 1.8 to 8.4 (Section 3.2.2). Chromite, present in the unaltered

261   material, did not dissolve during incubation while olivine completely dissolved in the pH_{14d} 1.8

262   and 2.2 samples as evident from the disappearance of its sharp diffraction peaks (Figure 2a,

263   Table 1).

264   *3.2.2. Mössbauer spectroscopy*

265   Mössbauer analysis of unaltered Adirondack basalt simulant showed that Fe was

266   associated with olivine and glass phases, 19 ± 2 and $81 \pm 2\%$ respectively and was mostly Fe(II)

267   (Table EA-2, (Peretyazhko et al., 2016)).

268   Analysis of altered Adirondack basalt simulant revealed formation of smectite through

269   alteration of the glass phase. The decrease in the concentration of total Fe associated with the

270   glass phase ($39 \pm 2\%$ pH_{14d} 3.1, $43 \pm 2\%$ pH_{14d} 3.7 and $54 \pm 2\%$ pH_{14d} 8.4, Figure 3a-c, Table

271   EA-2) compared to the unaltered simulant, was equal within error to amount of total Fe

272   associated with the smectite formed after 14d incubation (38 ± 2% pH_{14d} 3.1, 41 ± 2% pH_{14d} 3.7

273   and 56 ± 2% pH_{14d} 8.4, Figure 3a-c, Table EA-2). Smectite spectra were fit with one Fe(II)

274   doublet (CS = 1.04 -1.09 mm/s and QS = 2.42 -2.66 mm/s) and one Fe(III) doublet (CS = 0.41 -

275   0.48 mm/s and QS = 0.54 - 0.70 mm/s QS, Table EA-2) and assigned to Fe(II) and Fe(III) in

276   octahedral coordination (Treiman et al., 2014). The smectite was oxidized with Fe(III)/ΣFe equal

277   to 0.61, 0.73 and 0.82 at pH_{14d} 3.1, 3.7 and 8.4, respectively.

278   The most acidic pH_{14d} 1.8 sample was also characterized by Fe(II) and Fe(III) doublets

279   with parameters similar to those assigned to smectite in the other samples (Fe(II) doublet: CS =

280   1.03 mm/s and QS = 2.60 mm/s and Fe(III) doublet: CS = 0.46 mm/s and QS = 0.62 mm/s,

281   Table EA-2). However, smectite did not form in this sample within XRD detection limits (Table

282   1). The Fe might be associated with an altered glass layer which forms during first stage of acidic

283   basalt alteration (Berger et al., 1987; Oelkers, 2001) and/or with an incipient phyllosilicate with

284   domains too small to coherently scatter X-rays.

285   The concentration of total Fe associated with olivine progressively decreased with

286   decreasing pH_{14d}, and no Fe in olivine was detected in the pH_{14d} 1.8 sample as shown in Table

287   EA-2. Olivine dissolution by acid-sulfate solutions could contribute Fe to smectite precipitation.

288   However, the Mössbauer evidence is that Fe(II) from olivine dissolution was oxidized and

289   precipitated as hematite, because the decrease in concentration of Fe(II) associated with olivine

290   was associated with a concomitant increase in the concentration of Fe(III) associated with

291   hematite (Figure 3, Table EA-2). Iron content in hematite (15 ± 2% pH_{14d} 1.8, 12 ± 2% pH_{14d}

292   3.1, 8 ± 2% pH_{14d} 3.7 and 2 ± 2% pH_{14d} 8.4, Figure 3, Table EA-2), was equal within an error of

293   fitting to decrease in olivine Fe content with respect to the unaltered Adirondack basalt simulant

294   (19 ± 2% pH_{14d} 1.8, 11 ± 3% pH_{14d} 3.1, 6 ± 3% pH_{14d} 3.7 and 4 ± 3% pH_{14d} 8.4, Figure 3, Table

295 EA-2). The hematite peaks were broad and skewed toward zero velocity, implying poor

296 crystallinity (small particle diameter) and potentially Al substitution for Fe(III).

297 *3.2.3. Smectite composition and structural formula*

298 The structural formula calculated from electron microprobe analysis of smectite-containing

299 particles (Table EA-3, Figure EA-1) showed that smectite contained Si and Al in tetrahedral

300 layers, Al, Mg, Fe with traces of Ti, Mn, Ni and Cr in octahedral layers, and Na, Ca and K

301 occupied interlayer sites. Given the high uncertainties in the measured data due to high water

302 content in smectite, the results of electron microprobe analysis did not allow to accurately

303 quantify smectite composition. Electron microprobe analysis indicated that smectite enriched in

304 Fe and Mg formed at pH_{14d} 3.7, 7.2 and 8.4 while smectite equally enriched in Al, Mg and Fe

305 formed at pH_{14d} 3.1 (Table EA-3). The average total number of octahedral cations in a unit cell

306 was close to 6 in the pH_{14d} 3.7, 7.2 and 8.4 samples (Table EA-3) and was consistent with

307 trioctahedral saponite. The total number of octahedral cations was close to 5 in the pH_{14d} 3.1

308 sample (Table EA-3) which might indicate formation of smectite containing dioctahedral and

309 trioctahedral domains.

310 *3.2.4. Visible and near-infrared spectroscopy*

311 VNIR spectral features between ~1.2 and 2.5 μm (Figure 4, Table 2) for saponite formed

312 at pH_{14d} 3.7, 7.2, and 8.4 were assigned to OH in H_2O and M-OH (~1.4 μm), to interlayer and

313 adsorbed H_2O (~1.9 μm), and to trioctahedral M_3-OH and dioctahedral M_2-OH functional groups

314 (2.2-2.5 μm), where M is any combination of Al, Mg, Fe(II) and Fe(III) as octahedral cations.

315 The band centered between 2.30 and 2.32 μm was assigned to (Mg, Fe(II), Fe(III))$_3$OH

316 combination stretching and bending vibration (Neumann et al., 2011; Treiman et al., 2014). (Mg,

317 Fe(II), Fe(III))$_3$OH band center position was shifted to shorter wavelength in the pH_{14d} 8.4

318 sample with respect to the pH_{14d} 3.7 and 7.2 samples (Figure 4b, Table 2). The band position

319   shift could be due to increase in degree of Fe oxidation in saponite from Fe(III)/ΣFe = 0.73 at

320   pH_{14d} 3.7 to Fe(III)/ΣFe = 0.82 at pH_{14d} 8.4, (Table EA-2, (Peretyazhko et al., 2016)). The

321   position variability for the ~2.31 µm band might also result from heterogeneous distributions of

322   cations on octahedral sites [e.g., (Fe(III)$_2$Mg)-OH versus (Fe(III)Mg$_2$)-OH]. Saponite observed at

323   pH_{14d} 7.2 and 8.4 had a weaker band near 2.40 µm band commonly observed in Fe/Mg smectites

324   (e.g., Carter et al., 2015; Chemtob et al., 2015). The exact band assignment is uncertain but

325   might be due to (Mg, Fe(II), Fe(III))$_3$OH combination stretching and translation vibration (Frost

326   et al., 2002; Chemtob et al., 2015). The spectral feature near 2.24 µm was assigned to Al(Fe(III),

327   Fe(II), Mg)OH (Madejová et al., 2011; Chemtob et al., 2015) and indicated the presence of

328   octahedral Al, possibly present as dioctahedral domains as previously observed in synthetic

329   saponite (Chemtob et al., 2015; Peretyazhko et al., 2016). Spectral properties of saponite

330   synthesized at pH_{14d} 3.7, 7.2 and 8.4 were similar to the properties reported for smectite on Mars

331   by VNIR spectrometers. The bands near 2.30 and 2.40 µm has been reported in Fe/Mg-smectite

332   identified on Mars while the band at 2.24 µm is present in about 10% of Fe/Mg-phyllosilicate

333   spectra (Carter et al., 2013), including nontronite (Bishop et al., 2013) but not saponite.

334   The spectrum of the pH_{14d} 3.1 sample containing dioctahedral smectite was similar to the

335   spectra of the untreated Adirondack basalt simulant and pH_{14d} 1.8 and 2.2 samples (Figure 4b).

336   All these samples had a broad band centered on 2.21-2.22 µm likely resulting from vibration of

337   Si-OH associated with the unaltered glass phase. The diagnostic band of montmorillonite at 2.20

338   µm was not distinguishable from the basalt band because of relatively low smectite abundance at

339   pH_{14d} 3.1 (indicative by low intensity 001 diffraction peak in the sample, Figure 2a).

340   Hematite presence was evident from the ferric absorption edge between ~0.50 um and

341   ~0.75 um (Figure 4a) corresponding to the onset of strong absorption and a relative reflectivity

342   maximum for hematite (Morris et al., 1985). The VNIR manifestation of the hematite was most

343 noticeable for the pH_{14d} 1.8 sample which had the highest hematite content (15% of total Fe,

344 Table EA-2)

345 **3.3. Characterization of aqueous phase**

346 Mineralogical transformations of Adirondack basalt simulant to smectite, anhydrite,

347 hematite and natroalunite (Table 1) resulted in release of variable proportions of Si, Mg, Na and

348 Ca. Complete dissolution of olivine in the pH_{14d} 1.8 and 2.2 samples and subsequent release of

349 Mg and Si into solution (Figure 5a) were lower than the expected Si and Mg concentrations if all

350 olivine was dissolved (32 ± 3 mM Si and 42 ± 4 mM Mg based on the total SiO_2 and MgO

351 contents in olivine, Table EA-1). The results suggest that Si and Mg dissolved from olivine were

352 partially incorporated into an altered glass phase under acidic conditions (Berger et al., 1987).

353 Smectite formation in the pH_{14d} range from 3.1 to 8.4 (Figure 2a) led to decrease in Si

354 and Mg dissolution (Figure 5a) where the Mg dissolution likely controlled the nature of the

355 forming smectite mineral (Meunier, 2005). Dioctahedral smectite was only detected in the pH_{14d}

356 3.1 sample in which nearly 50% of the total Mg was leached into solution (calculations are based

357 on dissolved Mg concentrations in Figure 5a and total MgO in the glass phase, Table EA-1)

358 while formation of trioctahedral saponite (pH_{14d} 3.7, 7.2 and 8.4) was accompanied by lower or

359 no Mg release into solution.

360 Dissolved Na was affected by precipitation of natroalunite and smectite formation.

361 Dissolved Na concentration was low and did not change in the pH_{14d} range from 1.8 to 3.1 then

362 increased as pH shifted from acidic to slightly alkaline (Figure 5b). Low release of Na from

363 basaltic glass at pH_{14d} 1.8-3.1 could result from precipitation of natroalunite, although the

364 presence of this phase was only confirmed at pH_{14d} 1.8 (Table 1). Dissolved Na increased in the

365 pH_{14d} range from 3.1 to 8.4 (Figure 5b) due to Na loss from glass phase during alteration of

366 Adirondack basalt simulant into smectite (Peretyazhko et al., 2016). Similar to Na, Ca was

367   expected to increase in solution with increasing basalt alteration as pH rose (Berger et al., 1987).

368   However, dissolved Ca concentration did not change (Figure 5b), and such non-pH-dependent

369   Ca release, together with the observed decrease in sulfate concentration (Figure 5c), resulted

370   from anhydrite precipitation (Figure 2a, Table 1) which is favorable at elevated temperatures

371   (Bishop et al., 2014).

372   Solution concentrations of Al and Fe were low for all samples resulting from their

373   incorporation into secondary phases (Figure EA-4, Tables 1 and 2). Dissolved Al did not exceed

374   0.04 mM (Figure EA-4a) as a result of precipitation of natroalunite at pH_{14d} 1.8, low release from

375   glass alteration and incorporation into smectite at higher pH values (Tables 2 and EA-3) and

376   potentially in hematite. Dissolved Fe was <0.15 mM (Figure EA-4b) in all samples due to

377   precipitation of hematite accompanying olivine dissolution (Figure 3), low release from altering

378   glass phase and smectite formation (Tables 2 and EA-3).

379

380   **4. DISCUSSION**

381

382   The formation of smectite in the Noachian and early Hesperian has been attributed to

383   aqueous alteration of basaltic materials under neutral to alkaline pH aqueous conditions (Bibring

384   et al., 2006; Chevrier et al., 2007; Ehlmann et al., 2009; Bishop et al., 2013; Bristow et al., 2015;

385   Flahaut et al., 2015; Jain and Chauhan, 2015). However, the results of our experiments show that

386   formation of smectite from Mars-analogue basalt simulant is possible in much more acidic

387   environments. We found that gradual acid neutralization during acid-sulfate alteration of the

388   basalt simulant under hydrothermal conditions led to smectite formation at $pH_{14d} \geq 3$. The nature

389   of the forming smectite mineral varied with the solution final pH. Dioctahedral smectite equally

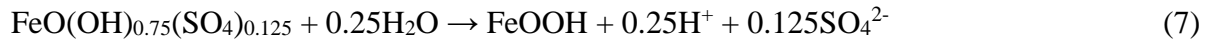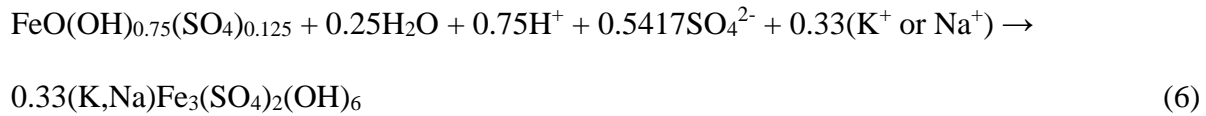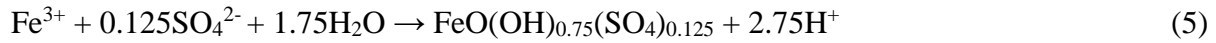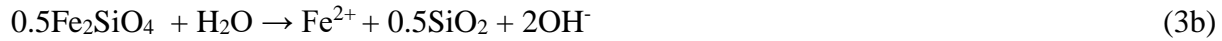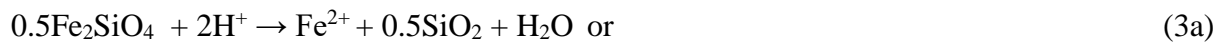390 enriched in Al, Fe and Mg formed at pH_{14d} ~3 followed by saponite enriched in Fe and Mg at

391 pH_{14d} close to 4 or higher.

392   Our experimental results demonstrate that smectite formation through basalt alteration on

393 Mars was not limited to neutral/alkaline pH conditions but could partially occur under acidic

394 conditions once solution pH was close to 3 or higher. Sources of acidity on early Mars and the

395 persistence of acidic aqueous environments have been controversial. The basaltic crust should

396 provide enormous acid neutralizing potential (Niles and Michalski, 2009) suggesting that

397 aqueous systems on Mars should be largely alkaline. However, as noted above, absence of large

398 scale carbonate deposits shows an evidence for acidic conditions even in heavily altered regions

399 of the martian crust (Fairén et al., 2004). The principal acidity sources proposed for early Mars

400 are Fe(II) oxidative hydrolysis (Tosca et al., 2008; Hurowitz et al., 2010) and SO_2 degassing

401 (Berger et al., 2009; Gaillard and Scaillet, 2009; Righter et al., 2009; Gaillard et al., 2013). We

402 argue here that SO_2 degassing was the major source of acidity on early Mars generating H_2SO_4

403 sufficient for acidic phyllosilicate formation through basalt alteration and Fe(II) oxidative

404 hydrolysis (i.e., Fe(III) hydrolysis) was likely not the source of wide-spread acidity on Mars.

405 **4.1. Acidity sources on early Mars: Fe(II) oxidative hydrolysis**

406   Iron(III) hydrolysis was first suggested as the source of acidity at Meridiani Planum

407 (Hurowitz et al., 2010) and was further generalized as a possible widespread acidity source on

408 early Mars (e.g., (Ehlmann et al., 2011; Bowen et al., 2012; Horgan and Bell III, 2012;

409 McLennan, 2012; Marlow et al., 2014; Kaplan et al., 2016)). The Fe(II) oxidative hydrolysis

410 model proposed that upwelling of anoxic Fe(II)-containing groundwater generated from basalt

411 dissolution under anoxic circum-neutral pH conditions could lead to surface oxidation of Fe(II)

412 to Fe(III) followed by Fe(III) hydrolysis, release of H^+ and precipitation of Fe(III) secondary

413   minerals (Hurowitz et al., 2010). The latter include nanophase iron(III) (hydr)oxides (interpreted

414   as schwertmannite ($FeO(OH)_{0.75}(SO_4)_{0.125}$) (Hurowitz et al., 2010)), jarosite

415   ($(K,Na)Fe_3(SO_4)_2(OH)_6$) and hematite (α-Fe_2O_3) detected by Mössbauer spectroscopy at

416   Meridiani Planum (Morris et al., 2006). The reactions below summarize the mechanism

417   proposed for acidity generation following the sequence developed by Hurowitz et al., (2010)

418   with the exception that eq. 3 is included for basalt dissolution (eq. 3 written for olivine Fe(II)-end

419   member fayalite (Fe_2SiO_4)):

420

421    $0.5Fe_2SiO_4 + 2H^+ \rightarrow Fe^{2+} + 0.5SiO_2 + H_2O$ or   (3a)

422    $0.5Fe_2SiO_4 + H_2O \rightarrow Fe^{2+} + 0.5SiO_2 + 2OH^-$ (3b)

423    $Fe^{2+} + 0.25O_2 + H^+ \rightarrow Fe^{3+} + 0.5H_2O$ (4)

424    $Fe^{3+} + 0.125SO_4^{2-} + 1.75H_2O \rightarrow FeO(OH)_{0.75}(SO_4)_{0.125} + 2.75H^+$ (5)

425    $FeO(OH)_{0.75}(SO_4)_{0.125} + 0.25H_2O + 0.75H^+ + 0.5417SO_4^{2-} + 0.33(K^+ \text{ or } Na^+) \rightarrow$

426    $0.33(K,Na)Fe_3(SO_4)_2(OH)_6$ (6)

427    $FeO(OH)_{0.75}(SO_4)_{0.125} + 0.25H_2O \rightarrow FeOOH + 0.25H^+ + 0.125SO_4^{2-}$ (7)

428    $FeOOH \rightarrow 0.5Fe_2O_3 + 0.5H_2O$ (8)

429   While groundwater interaction with basalt was suggested to be a source of dissolved

430   Fe(II), basalt dissolution (eq. 3) was not included into Fe(II) oxidative hydrolysis model

431   (Hurowitz et al., 2010). As a result, the model predicted that sufficient amount of H^+ was

432   produced through Fe(III) hydrolysis to develop acidic conditions (Hurowitz et al., 2010). If

433   basalt dissolution reactions are added to the model, then no acidity would be generated because

434   Fe(II) release is accompanied by OH^- release (e.g., eq. 3b, Text EA-1). While our calculations

435   only account for Fe, the release of Mg, Ca, and Na from the basalts will also be accompanied by

436   release of OH^- which will contribute to generation of additional alkalinity.

437   The OH^- generated from dissolution of basalt (eq. 3) could be neutralized by H^+ produced

438   through oxidative dissolution of Fe(II) sulfides present in basalt. However, the produced H^+ will

439   not be sufficient to neutralize all released OH^- on the basis of current estimates of low

440   abundances of Fe(II) sulfides in martian basalts (1600 mg/kg S in shergottite sulfides or 0.16

441   wt%, (Righter et al., 2009)). Alternatively, the OH^- released from basalt together with Fe(II),

442   Mg, Ca and Na could be neutralized if the anoxic alkaline solutions encounter anoxic acidic

443   solutions. If all released OH^- is neutralized, then Fe(II) oxidation followed by hydrolysis under

444   oxic conditions will lead to development of acidic conditions according to the Hurowitz et al.,

445   (2010) model (eqs. 4-8). However, such scenario will require presence of acidic conditions, for

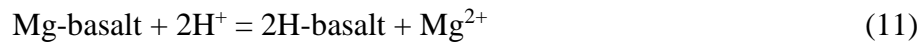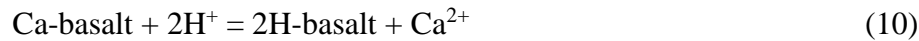446   instance H_2SO_4, before Fe(III) hydrolysis occurred.

447

448   **4.2. Acidity sources on early Mars: SO_2 degassing and H_2SO_4 formation**

449   Magmatic sulfur degassing was the dominant source for sulfates deposited on the surface

450   of Mars (Righter et al., 2009), but was SO_2 release on early Mars able to generate the amount of

451   H_2SO_4 sufficient for acidic phyllosilicate formation through alteration of basalt?

452   The calculated amount of sulfur release (eq. 2) during Noachian/early Hesperian epoch

453   was 2.5×10^{21} g [~4.5 Ga - ~3.4 Ga; an intermediate value of 3.4 Ga was used for early

454   Hesperian/Late Hesperian boundary which is around 3.2 Ga - 3.6 Ga (Hartmann, 2005); Figure

455   6]. If all sulfur was released as SO_2 and converted to H_2SO_4 then around 1.6×10^{20} moles of H^+

456   was produced during dissociation of all acid in water. Formation of sulfuric acid might occur

457   through disproportionation of SO_2 to H_2SO_4 and elemental S and S could be further transformed

458   into H_2SO_4 in the presence of oxidizing agent and water (Habashi and Bauer, 1966; Halevy et al.,

459   2007). It should be noted, however, an assumption that all degassed sulfur was transformed into

460   sulfuric acid likely overestimates the amount of produced acidity but our calculations allows to

461   potentially evaluate an upper limit of acidity that could have been generated on early Mars.

462   The protons generated from sulfuric acid are neutralized by Ca, Mg and Na in basalt via

463   proton exchange leading first to formation of an altered hydrated silica layer enriched in Fe and

464   Al (Berger et al., 1987; Peretyazhko et al., 2016) by schematic reactions:

465   Na-basalt + H^+ = H-basalt + Na^+ (9)

466   Ca-basalt + $2H^+$ = 2H-basalt + Ca^{2+} (10)

467   Mg-basalt + $2H^+$ = 2H-basalt + Mg^{2+} (11)

468   Crystallization of phyllosilicate from an altered layer does not substantially change pH as shown

469   in the previous studies of smectite formation through basalt alteration (Ghiara et al., 1993; De La

470   Fuente et al., 2002; Peretyazhko et al., 2016). Iron was not included into calculations because

471   overall process including dissolution of olivine followed by Fe(II) oxidation, Fe(III) hydrolysis

472   and hematite precipitation (Table 1) does not produce or consume H^+ (Text EA-1).

473   Approximately 9.4 mol_{H+}/kg_{basalt} H^+ is required for complete neutralization of Na, Ca and Mg in

474   basalt of Adirondack composition (Text EA-2). The amount of H^+ generated from volcanic

475   outgassing of SO_2 ($1.6x10^{20}$ moles) during the Noachian and Hesperian would be sufficient for

476   neutralization of Ca, Mg and Na along with phyllosilicate formation in a 42 m thick basalt layer

477   over the entire planet (Text EA-3). Given that formation of smectite requires Mg to be present in

478   the altering basalt (Kloprogge et al., 1999), partial H^+ neutralization by cations would be a more

479   realistic scenario on Mars. Noachian-aged terrains such as Mawrth Vallis have been estimated to

480   contain 20-65% smectite (Poulet et al., 2008). Assuming that the smectite abundance in Mawrth

481   Vallis is representative of H^+ neutralization and, consequently, degree of basalt alteration in

482   ancient martian terrains, the calculated average global depth of basaltic alteration would be

483   between 60 m (65% smectite content) to 200 m (20% smectite content) on the entire planet under

484   the constraint that alteration of 42 m thick basalt leads to 100% neutralization of Na, Ca and Mg.

485   The calculated depth range is consistent with phyllosilicate layer thickness of a few hundreds of

486   meters estimated in Noachian-aged terrains (Loizeau et al., 2012). Our acidity calculations and

487   experimental results, therefore, provide evidence that SO_2 degassing would result in production

488   of large amounts of H^+ and gradual neutralization of sulfuric acid during basalt alteration could

489   be an important mechanism of smectite formation on early Mars.

490

491   **5.   SIGNIFICANCE AND CONCLUSIONS**

492

493   Our experiments demonstrated formation of smectite through hydrothermal acid-sulfate

494   alteration of Mars-analogue glass-rich basalt (66 wt% glass, 32 wt% olivine and 2 wt%

495   chromite). Basalt simulant suspensions were acidic with initial $pH_{0d} \leq 2$ while final pH_{14d} varied

496   from acidic to mildly alkaline (pH_{14d} 1.8-8.4) at the end of 14d incubation at 200 °C. Alteration

497   of the glass phase of basalt simulant resulted in formation of dioctahedral smectite as pH_{14d}

498   reached ~3 followed by trioctahedral saponite at pH_{14d} close to 4 or higher. Reaction of

499   Adirondack basalt simulant with sulfuric acid also led to formation of anhydrite at all pH_{14d}

500   values while natroalunite was detected at pH_{14d} 1.8. Hematite precipitated as a result of partial or

501   complete oxidative dissolution of olivine in the pH_{14d} range from 1.8 to 8.4.

502   Acidity on early Mars can be accounted for by volcanic outgassing of SO_2 and formation

503   of sulfuric acid. Acid-sulfate conditions, suitable enough to form smectite and prevent carbonate

504   formation were likely sustained by low water/rock ratio and short duration of water-rock

505   interaction (Berger et al., 2009; Berger et al., 2014). Acidic smectite formation areas on early

506   Mars might be constrained to near-surface hydrothermal areas with magmatic outgassing

507   resulted from volcanic or impact activity (Solomon et al., 2005; Hynek et al., 2013). In these

508   systems only small portions of crust are exposed to acidity generated by H_2SO_4 formed from

509   degassed SO_2. Short-term aquatic systems analogous to ephemeral acid saline lakes in Western

510   Australia might also allow development of acidic conditions (Story et al., 2010; Bowen et al.,

511   2012). Although there may also be acidity generated by the Fe(II) oxidative hydrolysis in local

512   environments, our calculations indicate that this mechanism is not a plausible large-scale acidity

513   source because of the alkalinity that is generated during basalt dissolution.

514   Formation of phyllosilicate by sulfuric acid alteration of basaltic materials on Mars would

515   likely be accompanied by precipitation of sulfate minerals including anhydrite. Although

516   anhydrite cannot be detected by the same remote sensing measurements used to detect

517   phyllosilicates because of the absence of diagnostic H_2O spectral features in the VNIR, anhydrite

518   might coprecipitate with phyllosilicate in deposits formed under hydrothermal sulfuric acid

519   environments (>60 °C (Bishop et al., 2014)). Acid-sulfate smectite formation might also occur in

520   younger terrains. Phyllosilicates (e.g., smectite) co-existing with anhydrite in Gale crater may

521   have formed along with the anhydrite under acid sulfate conditions (Rampe et al., 2017). The

522   hypothesis is supported by occurrence of jarosite in these mudstones in Gale crater indicative of

523   acidic environments (Rampe et al., 2017). Fe/Mg-rich phyllosilicates interbedded with sulfate

524   minerals in Meridiani Planum have been proposed to form prior to sulfates in moderate pH,

525   sulfate-free aqueous environments followed by sulfate precipitation from acidic surface and

526   groundwater (Flahaut et al., 2015). Our findings demonstrate that multiple events are not

527   required to form interbedded phyllosilicates and sulfates deposits. Acid-sulfate alteration can

528   explain martian mineralogical observations including mixed phyllosilicate/sulfate deposits and

529   lack of abundant carbonate deposits.

530

531

ACKNOWLEDGEMENTS

556   **REFERENCES**

557

558   Abdelouas A., Crovisier J.-L., Lutze W., Grambow B., Dran J.-C. and Müller R. (1997) Surface

559   layers on a borosilicate nuclear waste glass corroded in $MgCl_2$ solution. *J. Nucl. Mater.* **240**,

560   100-111.

561   Agresti D. G., Dyar M. D. and Schaefer M. W. (2007) Velocity scales for Mars Mössbauer data.

562   *NASSAU 2006*, 67-74.

563   Agresti D. G. and Gerakines P. A. (2009) Simultaneous fitting of Mars Mössbauer data. *ICAME*

564   *2007*, 1347-1354.

565   Bain D. C. and Smith B. F. L. (1987) Chemical analysis, In: *A handbook of determinative*

566   *methods in clay mineralogy* (ed. M. J. Wilson). Chapman and Hall, New York, pp. 248-275.

567   Berger G., Meunier A. and Beaufort D. (2014) Clay mineral formation on Mars: Chemical

568   constraints and possible contribution of basalt out-gassing. *Planet. Space Sci.* **95**, 25-32.

569   Berger G., Schott J. and Loubet M. (1987) Fundamental processes controlling the first stage of

570   alteration of a basalt glass by seawater: an experimental study between 200 and 320 C. *Earth.*

571   *Planet. Sci. Lett.* **84**, 431-445.

572   Berger G., Toplis M. J., Treguier E., d'Uston C. and Pinet P. (2009) Evidence in favor of small

573   amounts of ephemeral and transient water during alteration at Meridiani Planum, Mars. *Am.*

574   *Mineral.* **94**, 1279-1282.

575   Bibring J.-P., Langevin Y., Mustard J. F., Poulet F., Arvidson R., Gendrin A., Gondet B.,

576   Mangold N., Pinet P. and Forget F. (2006) Global mineralogical and aqueous Mars history

577   derived from OMEGA/Mars Express data. *Science* **312**, 400-404.

578   Bishop J. L., Lane M. D., Dyar M. D., King S. J., Brown A. J. and Swayze G. A. (2014) What

579   lurks in the martian rocks and soil? Investigations of sulfates, phosphates, and perchlorates.

580   Spectral properties of Ca-sulfates: gypsum, bassanite, and anhydrite. *Am. Mineral.* **99**, 2105-

581   2115.

582   Bishop J. L., Loizeau D., McKeown N. K., Saper L., Dyar M. D., Des Marais D. J., Parente M.

583   and Murchie S. L. (2013) What the ancient phyllosilicates at Mawrth Vallis can tell us about

584   possible habitability on early Mars. *Planet. Space Sci.* **86**, 130-149.

585   Bowen B. B., Benison K. C. and Story S. (2012) Early diagenesis by modern acid brines in

586   Western Australia and implications for the history of sedimentary modification on Mars. *Mars*

587   *Sedimentology, SEPM Special Publication* **102**, 229-252.

588   Bristow T. F., Bish D. L., Vaniman D. T., Morris R. V., Blake D. F., Grotzinger J. P., Rampe E.

589   B., Crisp J. A., Achilles C. N. and Ming D. W. (2015) The origin and implications of clay

590   minerals from Yellowknife Bay, Gale crater, Mars. *Am. Mineral.* **100**, 824-836.

591   Carter J., Poulet F., Bibring J. P., Mangold N. and Murchie S. (2013) Hydrous minerals on Mars

592   as seen by the CRISM and OMEGA imaging spectrometers: Updated global view. *J. Geophys.*

593   *Res. Planets* **118**, 831-858.

594   Cavanagh P. D., Bish D. L., Blake D. F., Vaniman D. T., Morris R. V., Ming D. W., Rampe E.

595   B., Achilles C. N., Chipera S. J., Treiman A. H., Downs R. T. and Morrison S. M. (2015)

596   Confidence Hills mineralogy and CheMin results from base of Mt. Sharp, Pahrump Hills, Gale

597   Crater, Mars LPSC.

598   Chemtob S. M., Nickerson R. D., Morris R. V., Agresti D. G. and Catalano J. G. (2015)

599   Synthesis and structural characterization of ferrous trioctahedral smectites: Implications for clay

600   mineral genesis and detectability on Mars. *J.Geophys. Res. Planets*. **120**, 1119 -1140

601   Chevrier V., Poulet F. and Bibring J.-P. (2007) Early geochemical environment of Mars as

602   determined from thermodynamics of phyllosilicates. *Nature* **448**, 60-63.

603   Craddock R. A. and Greeley R. (2009) Minimum estimates of the amount and timing of gases

604   released into the martian atmosphere from volcanic eruptions. *Icarus* **204**, 512-526.

605   De La Fuente S., Cuadros J. and Linares J. (2002) Early stages of volcanic tuff alteration in

606   hydrothermal experiments: formation of mixed-layer illite-smectite. *Clays Clay Miner.* **50**, 578-

607   590.

608   Dehouck E., Gaudin A., Mangold N., Lajaunie L., Dauzères A., Grauby O. and Le Menn E.

609   (2014) Weathering of olivine under CO_2 atmosphere: a martian perspective. *Geochim.*

610   *Cosmochim. Acta* **135**, 170-189.

611   Edwards C. S. and Ehlmann B. L. (2015) Carbon sequestration on Mars. *Geo* **43**, 863-866.

612   Ehlmann B. L., Mustard J. F., Murchie S. L., Bibring J.-P., Meunier A., Fraeman A. A. and

613   Langevin Y. (2011) Subsurface water and clay mineral formation during the early history of

614   Mars. *Nature* **479**, 53-60.

615   Ehlmann B. L., Mustard J. F., Murchie S. L., Poulet F., Bishop J. L., Brown A. J., Calvin W. M.,

616   Clark R. N., Des Marais D. J. and Milliken R. E. (2008) Orbital identification of carbonate-

617   bearing rocks on Mars. *Science* **322**, 1828-1832.

618   Ehlmann B. L., Mustard J. F., Swayze G. A., Clark R. N., Bishop J. L., Poulet F., Des Marais D.

619   J., Roach L. H., Milliken R. E. and Wray J. J. (2009) Identification of hydrated silicate minerals

620   on Mars using MRO-CRISM: Geologic context near Nili Fossae and implications for aqueous

621   alteration. *J. Geophys. Res. Planets* **114**.

622   Fairén A. G. (2013) Coeval synthesis of cold aqueous mineralogies on Mars, In: *Mars: evolution,*

623   *geology and exploration* (ed. A. G. Fairén). Nova Science Publisher.

624   Fairén A. G., Fernández-Remolar D., Dohm J. M., Baker V. R. and Amils R. (2004) Inhibition

625   of carbonate synthesis in acidic oceans on early Mars. *Nature* **431**, 423-426.

626   Farrand W. H., Glotch T. D., Rice J. W., Hurowitz J. A. and Swayze G. A. (2009) Discovery of

627   jarosite within the Mawrth Vallis region of Mars: Implications for the geologic history of the

628   region. *Icarus* **204**, 478-488.

629   Flahaut J., Carter J., Poulet F., Bibring J.-P., van Westrenen W., Davies G. and Murchie S.

630   (2015) Embedded clays and sulfates in Meridiani Planum, Mars. *Icarus* **248**, 269-288.

631 Frost R. L., Kloprogge J. T. and Ding Z. (2002) Near-infrared spectroscopic study of nontronites

632 and ferruginous smectite. *Spectrochim. Acta* **58**, 1657-1668.

633 Gaillard F., Michalski J., Berger G., McLennan S. M. and Scaillet B. (2013) Geochemical

634 reservoirs and timing of sulfur cycling on Mars. *Space Sci. Rev.* **174**, 251-300.

635 Gaillard F. and Scaillet B. (2009) The sulfur content of volcanic gases on Mars. *Earth. Planet.*

636 *Sci. Lett.* **279**, 34-43.

637 Ghiara M., Franco E., Petti C., Stanzione D. and Valentino G. (1993) Hydrothermal interaction

638 between basaltic glass, deionized water and seawater. *Chem. Geol.* **104**, 125-138.

639 Greeley R. and Schneid B. (1991) Magma generation on Mars- Amounts, rates, and

640 comparisons with earth, moon, and Venus. *Science* **254**, 996-998.

641 Habashi F. and Bauer E. (1966) Aqueous oxidation of elemental sulfur. *Ind. Eng. Chem.*

642 *Fundam.* **5**, 469-471.

643 Halevy I., Zuber M. T. and Schrag D. P. (2007) A sulfur dioxide climate feedback on early

644 Mars. *Science* **318**, 1903-1907.

645 Hartmann W. K. (2005) Martian cratering 8: Isochron refinement and the chronology of Mars.

646 *Icarus* **174**, 294-320.

647 Haymon R. M. and Kastner M. (1986) The formation of high temperature clay minerals from

648 basalt alteration during hydrothermal discharge on the East Pacific Rise axis at 21 N. *Geochim.*

649 *Cosmochim. Acta* **50**, 1933-1939.

650 Hirschmann M. M. and Withers A. C. (2008) Ventilation of CO_2 from a reduced mantle and

651 consequences for the early Martian greenhouse. *Earth. Planet. Sci. Lett.* **270**, 147-155.

652 Horgan B. and Bell III J. F. (2012) Widespread weathered glass on the surface of Mars. *Geology*

653 **40**, 391-394.

654 Hurowitz J. A., Fischer W. W., Tosca N. J. and Milliken R. E. (2010) Origin of acidic surface

655 waters and the evolution of atmospheric chemistry on early Mars. *Nat. Geosci.***3**, 323-326.

656 Hynek B. M., McCollom T. M., Marcucci E. C., Brugman K. and Rogers K. L. (2013)

657 Assessment of environmental controls on acid-sulfate alteration at active volcanoes in

658 Nicaragua: Applications to relic hydrothermal systems on Mars. *J. Geophys. Res. Planets* **118**,

659 2083-2104.

660 Jain N. and Chauhan P. (2015) Study of phyllosilicates and carbonates from the Capri Chasma

661 region of Valles Marineris on Mars based on Mars Reconnaissance Orbiter-Compact

662 Reconnaissance Imaging Spectrometer for Mars (MRO-CRISM) observations. *Icarus* **250**, 7-17.

663 Kachanoski R., Voroney R. and Gregorich E. (1988) Ultrasonic dispersion of aggregates:

664 distribution of organic matter in size fractions. *Can. J. Soil. Sci.* **68**, 395-403.

665 Kaplan H. H., Milliken R. E., Fernández-Remolar D., Amils R., Robertson K. and Knoll A. H.

666 (2016) Orbital evidence for clay and acidic sulfate assemblages on Mars based on mineralogical

667 analogs from Rio Tinto, Spain. *Icarus* **275**, 45-64.

668   Klingelhoefer G., Morris R. V., Bernhardt B., Rodionov D., De Souza P., Squyres S., Foh J.,

669   Kankeleit E., Bonnes U. and Gellert R. (2003) Athena MIMOS II Mössbauer spectrometer

670   investigation. *J. Geophys. Res. Planets* **108**.

671   Kloprogge J. T., Komarneni S. and Amonette J. E. (1999) Synthesis of smectite clay minerals: a

672   critical review. *Clays Clay Miner.* **47**, 529-554.

673   Loizeau D., Werner S., Mangold N., Bibring J.-P. and Vago J. (2012) Chronology of deposition

674   and alteration in the Mawrth Vallis region, Mars. *Planet. Space Sci.* **72**, 31-43.

675   Madejová J., Balan E. and Petit S. (2011) Application of vibrational spectroscopy to the

676   characterization of phyllosilicates and other industrial minerals. *Advances in the*

677   *Characterization of Industrial Minerals: Notes in Mineralogy* **9**, 171-226.

678   Marlow J. J., LaRowe D. E., Ehlmann B. L., Amend J. P. and Orphan V. J. (2014) The potential

679   for biologically catalyzed anaerobic methane oxidation on ancient Mars. *Astrobiology* **14**, 292-

680   307.

681   McLennan S. M. (2012) Geochemistry of sedimentary processes on Mars. *Sediment. Geol.Mars*

682   **102**, 119-138.

683   McMurtry G. M. and Yeh H.-W. (1981) Hydrothermal clay mineral formation of East Pacific

684   Rise and Bauer Basin sediments. *Chem. Geol.* **32**, 189-205.

685 McSween H. Y., Wyatt M. B., Gellert R., Bell J., Morris R. V., Herkenhoff K. E., Crumpler L.

686 S., Milam K. A., Stockstill K. R. and Tornabene L. L. (2006) Characterization and petrologic

687 interpretation of olivine-rich basalts at Gusev Crater, Mars. *J. Geophys. Res. Planets* **111**.

688 Meunier A. (2005) *Clays*. Springer Science & Business Media.

689 Milliken R., Fischer W. and Hurowitz J. (2009) Missing salts on early Mars. *Geophys. Res. Lett.*

690 **36**.

691 Moore D. M. and Reynolds R. C. J. (1997) *X-ray diffraction and the identification and analysis*

692 *of clay minerals*. Oxford University Press, New York.

693 Morris R. V., Golden D., Bell J. F. and Lauer H. (1995) Hematite, pyroxene, and phyllosilicates

694 on Mars: Implications from oxidized impact melt rocks from Manicouagan Crater, Quebec,

695 Canada. *J. Geophys. Res. Planets* **100**, 5319-5328.

696 Morris R. V., Klingelhoefer G., Schröder C., Rodionov D. S., Yen A., Ming D. W., De Souza P.,

697 Wdowiak T., Fleischer I. and Gellert R. (2006) Mössbauer mineralogy of rock, soil, and dust at

698 Meridiani Planum, Mars: Opportunity's journey across sulfate-rich outcrop, basaltic sand and

699 dust, and hematite lag deposits. *J. Geophys. Res. Planets* **111**.

700 Morris R. V., Lauer H. V., Lawson C. A., Gibson E. K., Nace G. A. and Stewart C. (1985)

701 Spectral and other physicochemical properties of submicron powders of hematite (α-Fe_2O_3),

702 maghemite (γ-Fe_2O_3), magnetite (Fe_3O_4), goethite (α-FeOOH), and lepidocrocite (γ-FeOOH). *J.*

703 *Geophys. Res. Solid Earth* **90**, 3126-3144.

704 Morris R. V., Ruff S. W., Gellert R., Ming D. W., Arvidson R. E., Clark B. C., Golden D.,

705 Siebach K., Klingelhöfer G. and Schröder C. (2010) Identification of carbonate-rich outcrops on

706 Mars by the Spirit rover. *Science* **329**, 421-424.

707 Murchie S. L., Mustard J. F., Ehlmann B. L., Milliken R. E., Bishop J. L., McKeown N. K., Noe

708 Dobrea E. Z., Seelos F. P., Buczkowski D. L. and Wiseman S. M. (2009) A synthesis of Martian

709 aqueous mineralogy after 1 Mars year of observations from the Mars Reconnaissance Orbiter. *J.*

710 *Geophys. Res. Planets* **114**.

711 Neumann A., Petit S. and Hofstetter T. B. (2011) Evaluation of redox-active iron sites in

712 smectites using middle and near infrared spectroscopy. *Geochim. Cosmochim. Acta* **75**, 2336-

713 2355.

714 Niles P. B., Catling D. C., Berger G., Chassefière E., Ehlmann B. L., Michalski J. R., Morris R.,

715 Ruff S. W. and Sutter B. (2013) Geochemistry of carbonates on Mars: implications for climate

716 history and nature of aqueous environments. *Space Scie. Rev.* **174**, 301-328.

717 Niles P. B. and Michalski J. (2009) Meridiani Planum sediments on Mars formed through

718 weathering in massive ice deposits. *Nat. Geosci.* **2**, 215-220.

719 Oelkers E. H. (2001) General kinetic description of multioxide silicate mineral and glass

720 dissolution. *Geochim. Cosmochim. Acta* **65**, 3703-3719.

721 Peretyazhko T., Sutter B., Morris R., Agresti D., Le L. and Ming D. (2016) Fe/Mg smectite

722 formation under acidic conditions on early Mars. *Geochim. Cosmochim. Acta* **173**, 37-49.

723   Poulet F., Bibring J.-P., Mustard J., Gendrin A., Mangold N., Langevin Y., Arvidson R., Gondet

724   B., Gomez C. and Berthé M. (2005) Phyllosilicates on Mars and implications for early Martian

725   climate. *Nature* **438**, 623-627.

726   Poulet F., Mangold N., Loizeau D., Bibring J.-P., Langevin Y., Michalski J. and Gondet B.

727   (2008) Abundance of minerals in the phyllosilicate-rich units on Mars. *Astron.Astrophys.* **487**,

728   L41-L44.

729   Rampe E. B., Ming D. W., Blake D. F., Bristow T. F., Chipera S. J., Grotzinger J. P., Morris R.

730   V., Morrison S. M., Vaniman D. T., Yen A. S. and et al (2017) Mineralogy of an ancient

731   lacustrine mudstone succession from the Murray formation, Gale

732   crater, Mars. *Earth. Planet. Sci. Lett.* **471,** 172-185.

733   Righter K., Pando K. and Danielson L. (2009) Experimental evidence for sulfur-rich martian

734   magmas: Implications for volcanism and surficial sulfur sources. *Earth. Planet. Sci. Lett.* **288**,

735   235-243.

736   Seyfried W., Shanks W. and Dibble W. (1978) Clay mineral formation in DSDP Leg 34 basalt.

737   *Earth. Planet. Sci. Lett.* **41**, 265-276.

738   Solomon S. C., Aharonson O., Aurnou J. M., Banerdt W. B., Carr M. H., Dombard A. J., Frey H.

739   V., Golombek M. P., Hauck S. A. and Head J. W. (2005) New perspectives on ancient Mars.

740   *Science* **307**, 1214-1220.

741   Story S., Bowen B. B., Benison K. C. and Schulze D. G. (2010) Authigenic phyllosilicates in

742   modern acid saline lake sediments and implications for Mars. *J. Geophys. Res. Planets* **115**.

743   Tosca N. J., McLennan S. M., Dyar M. D., Sklute E. C. and Michel F. M. (2008) Fe oxidation

744   processes at Meridiani Planum and implications for secondary Fe mineralogy on Mars. *J.*

745   *Geophys. Res. Planets* **113**.

746   Treiman A. H., Morris R. V., Agresti D. G., Graff T. G., Achilles C. N., Rampe E. B., Bristow T.

747   F., Blake D. F., Vaniman D. T. and Bish D. L. (2014) Ferrian saponite from the Santa Monica

748   Mountains (California, USA, Earth): Characterization as an analog for clay minerals on Mars

749   with application to Yellowknife Bay in Gale Crater. *Am. Mineral.* **99**, 2234-2250.

750   Vaniman D., Bish D., Ming D., Bristow T., Morris R., Blake D., Chipera S., Morrison S.,

751   Treiman A. and Rampe E. (2014) Mineralogy of a mudstone at Yellowknife Bay, Gale crater,

752   Mars. *Science* **343**, 1243480.

753   Whittig L. D. and Allardice W. R. (1986) X-ray diffraction techniques, In: *Methods of soil*

754   *analysis. Part 1 Physical and mineralogical methods* (ed. A. Klute). American Society of

755   Agronomy, Madison, pp. 331-363.

756   Wray J., Milliken R., Dundas C., Swayze G., Andrews-Hanna J., Baldridge A., Chojnacki M.,

757   Bishop J., Ehlmann B. and Murchie S. L. (2011) Columbus crater and other possible

758   groundwater-fed paleolakes of Terra Sirenum, Mars. *J. Geophys. Res. Planets* **116**.

759   Wray J. J., Murchie S. L., Bishop J. L., Ehlmann B. L., Milliken R. E., Wilhelm M. B., Seelos K.

760   D. and Chojnacki M. (2016) Orbital evidence for more widespread carbonate-bearing rocks on

761   Mars. *J. Geophys. Res. Planets* **121**, 652-677.

762   Zolotov M. Y. and Mironenko M. V. (2007) Timing of acid weathering on Mars: A

763   kinetic-thermodynamic assessment. *J. Geophys. Res. Planets* **112**.

764   Zolotov M. Y. and Mironenko M. V. (2016) Chemical models for martian weathering profiles:

765   Insights into formation of layered phyllosilicate and sulfate deposits. *Icarus* **275**, 203-220.

766

767

768

769   Table 1. Phases determined in the 14d-incubated Adirondack basalt simulants by XRD and

770   Mössbauer spectroscopy. Olivine and chromite are unaltered phases from the original basalt

771   simulant.

pH_{14d}	Crystalline phases
1.81 ± 0.01	anhydrite, natroalunite, hematite[a], chromite
2.19 ± 0.01	anhydrite, chromite
3.12 ± 0.03	dioctahedral smectite, anhydrite, hematite, olivine, chromite
3.72 ± 0.34	saponite, anhydrite, hematite, olivine, chromite
7.17 ± 0.38	saponite, anhydrite, olivine, chromite
8.38 ± 0.20	saponite, anhydrite, hematite, olivine, chromite

772   [a]Hematite was detected by both XRD and Mössbauer in the pH_{14d} 1.8 sample and by Mössbauer
773   spectroscopy alone in the other samples. Hematite was present within the pH_{14d} range from 1.8 to
774   8.4 and likely precipitated in the pH_{14d} 2.2 and 7.2 samples not analyzed by Mössbauer
775   spectroscopy.

776

777

778

779

780

781

782

783

784

785

786

787

788

789

790   Table 2. Smectite characterization data obtained by XRD and VNIR.

pH_{14d}	Smectite	XRD d-spacing, Å		VNIR combination band position, μm		
		02*l*	060	Al(Fe(III), Fe(II), Mg)OH[b]	(Mg, Fe(II), Fe(III))$_3$OH[b]	(Mg, Fe(II), Fe(III))$_3$OH[c]
3.12 ± 0.03	dioctahedral smectite	4.48	1.50	nd[a]	nd	nd
3.72 ± 0.34	saponite	4.55	1.53	2.239	2.319	nd
7.17 ± 0.38	saponite	4.58	1.53	2.246	2.319	2.403
8.38 ± 0.20	saponite	4.57	1.53	2.243	2.300	2.408

791   [a] nd-not detected; [b] Combination stretching and bending vibration (Neumann et al., 2011;
792   Treiman et al., 2014); [c] Combination stretching and translation vibration (Frost et al., 2002;
793   Chemtob et al., 2015).
794

795

796

797

798
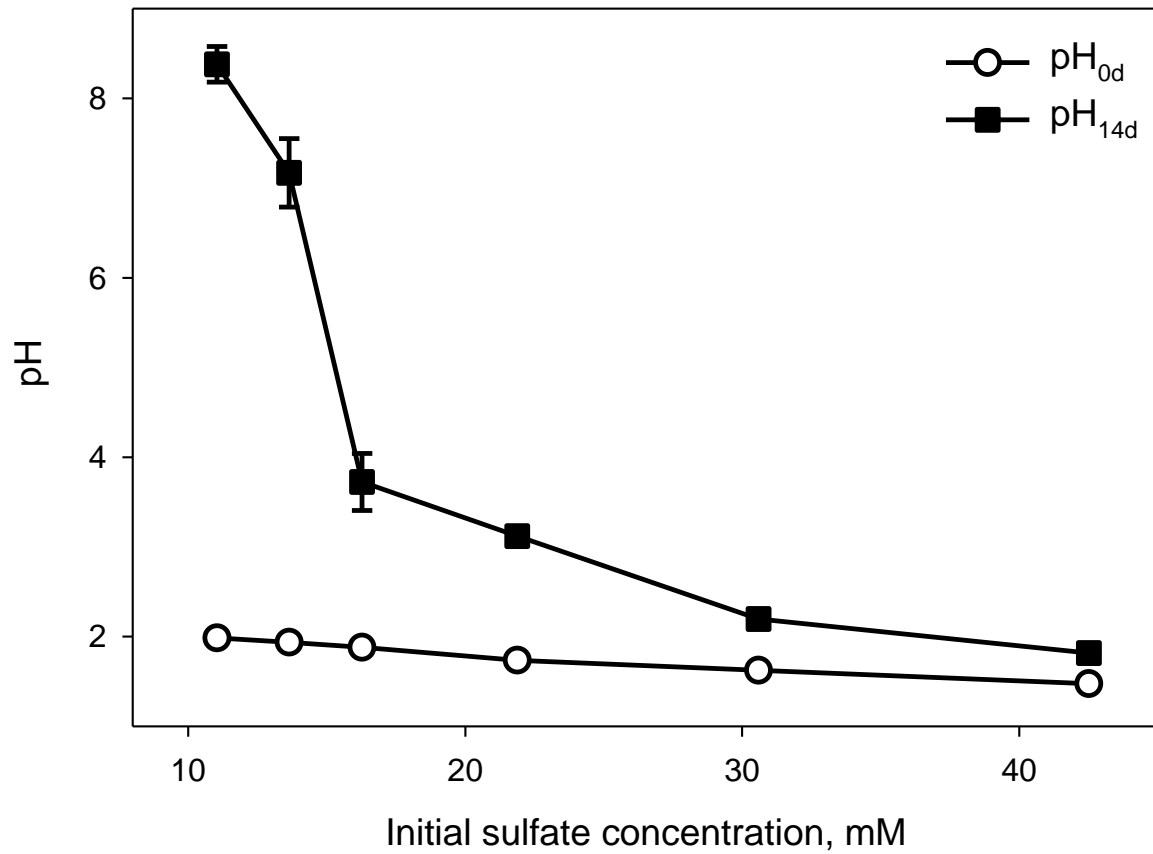
799
800
801 Figure 1. Initial (pH_{0d}) and final (pH_{14d}) pH in Adirondack basalt simulant suspensions as a
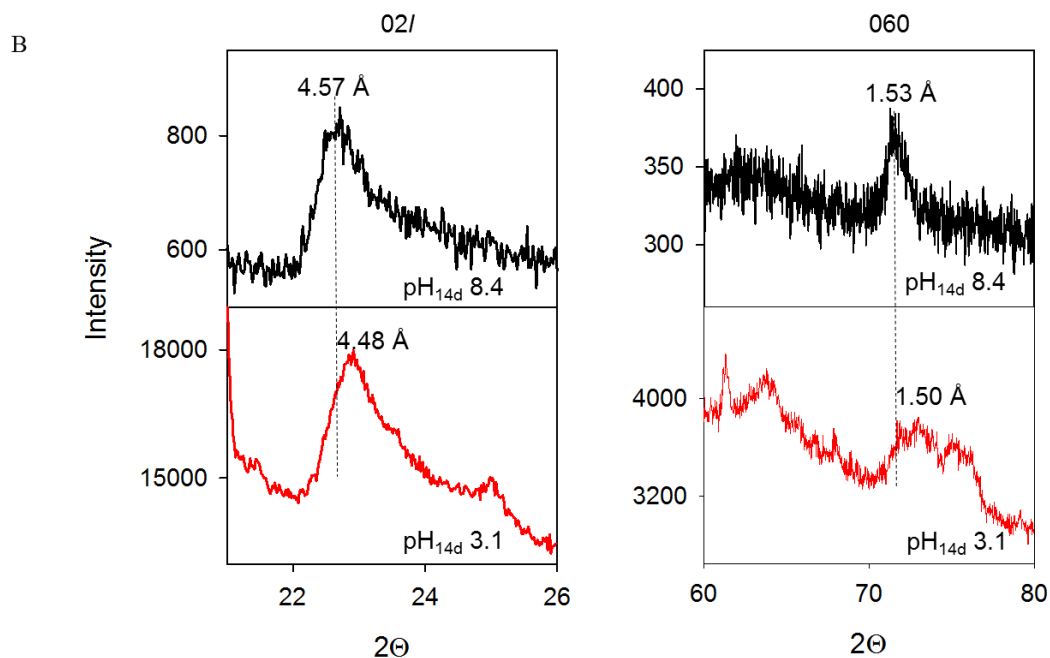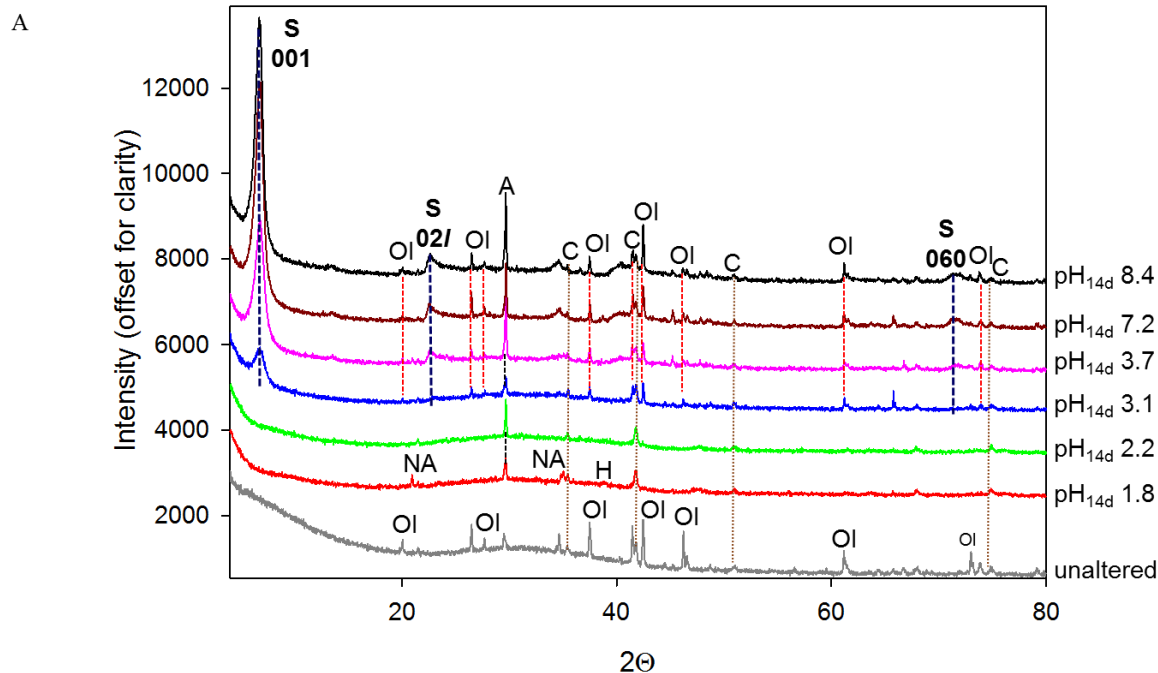802 function of initial sulfate concentrations.
803

Figure 2. (a) XRD for unaltered and 14d-incubated Adirondack basalt simulant samples with
different pH$_{14d}$. S = smectite (001, 02l and 060 diffraction peaks are marked next to or above the
peaks), A = anhydrite, Ol = olivine, C = chromite, NA = natroalunite, H = hematite; (b) 02l and
060 diffraction bands for clay fractions separated from the pH$_{14d}$ 8.4 and 3.1 samples. The bands
were analyzed with a 0.02° 2θ step for 1 min and 0.02° 2θ step for 17 min in the pH$_{14d}$ 8.4 and
3.1 clay fractions, respectively.

811
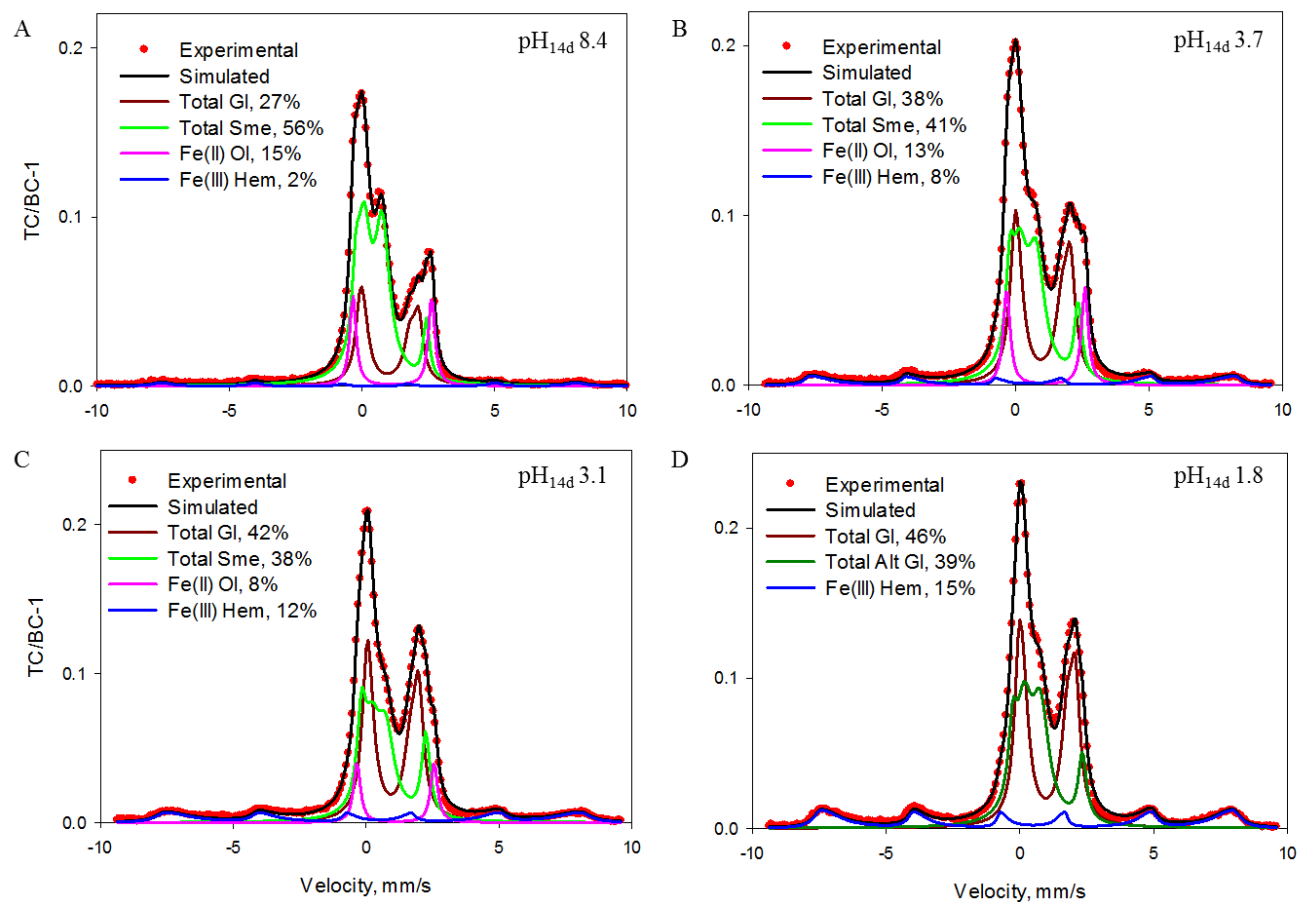
Figure 3. Mössbauer spectra and fit subspectra for 14d-incubated (a) pH_{14d} 8.4, (b) pH_{14d} 3.7, (c) pH_{14d} 3.1 and (d) pH_{14d} 1.8 Adirondack basalt simulant collected at RT [subspectral areas in % are for Ol = olivine; Total Gl = total glass, a sum of 2D1 and 2D2 doublets (Table EA-2), Total Sme = total smectite, and Total Alt Gl = total altered glass, a sum of 3D2 and 2D4 doublets (Table EA-2)]. TC = total counts, BC = baseline counts.
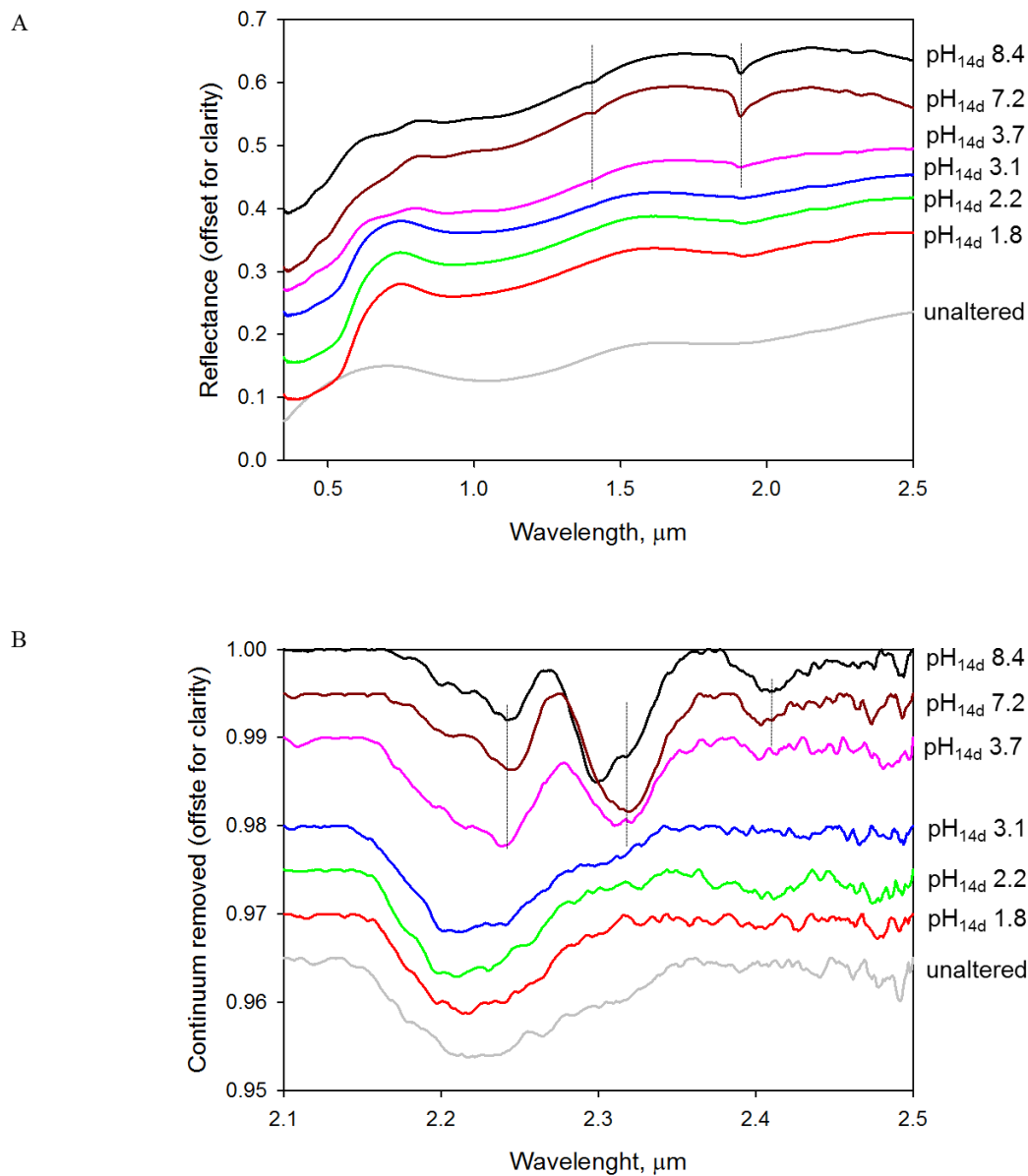
A

B

Figure 4. (a) VNIR reflectance spectra of unaltered and 14d-incubated Adirondack basalt simulant samples with different pH_{14d}. Bands at 1.4 and 1.9 µm in the saponite-containing pH_{14d} 8.4, 7.2 and 3.7 samples are marked with dotted lines. (b) 2-2.5 µm range of continuum removed reflectance spectra. Positions of M_3-OH and M_2-OH combination bands in the saponite-containing samples are marked with dotted lines (M is any combination of Al, Mg, Fe(II) and Fe(III) as octahedral cations). Characteristic Al_2OH band of montmorillonite at 2.21 µm in the pH_{14d} 3.1 sample was not detected.
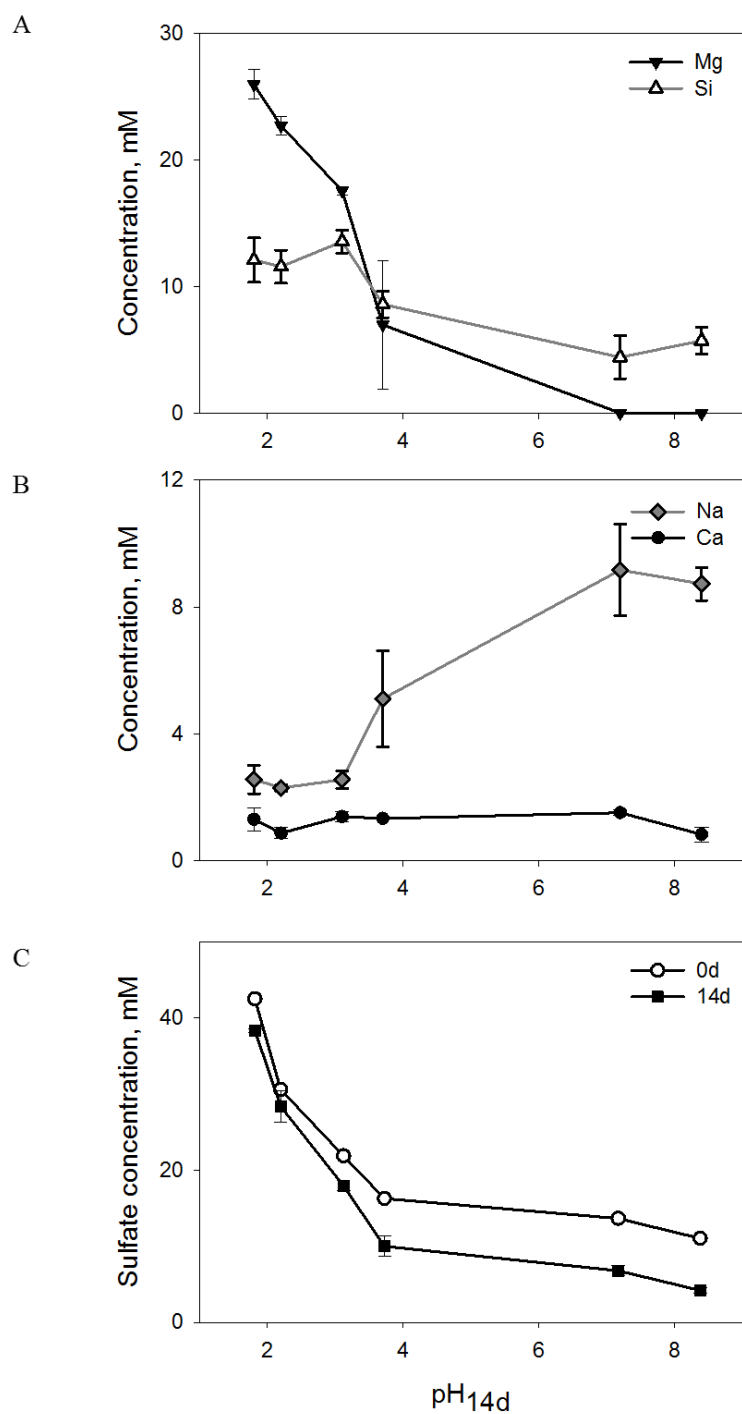
824

825

826   Figure 5. Concentrations of dissolved (a) Mg and Si, (b) Na and Ca and (c) sulfate in Adirondack
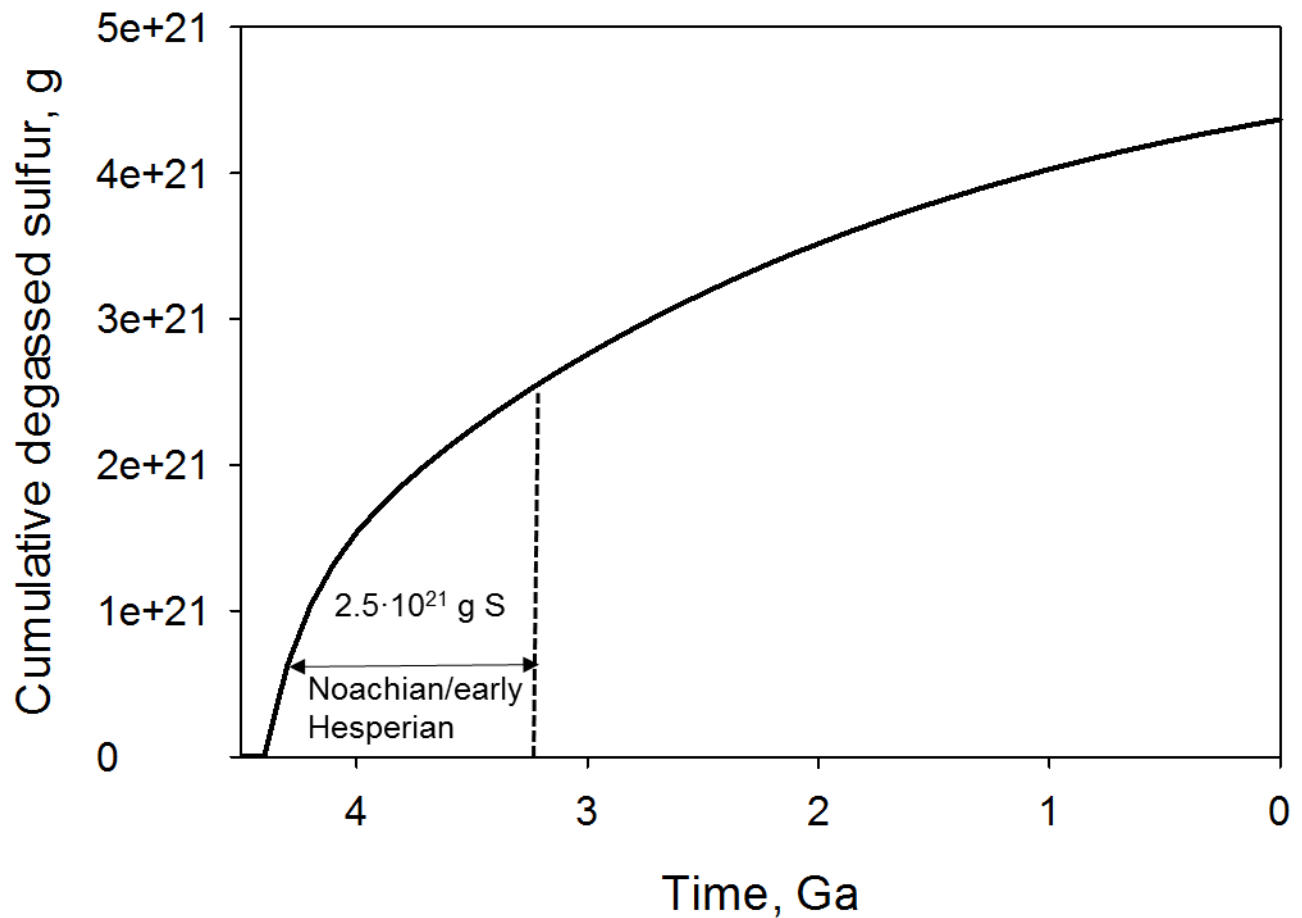827   basalt simulant suspensions as a function of pH_{14d}.

828

42

830 Figure 6. Sulfur degassed on Mars from 4.5 Ga to present calculated using the crust production
831 model (eq. 2, Hirschmann and Withers 2008) and amount of sulfur degassed from 1 kg magma
832 (2400 mg/kg, Righter et al., 2009). The calculated total degassed sulfur from 4.5 Ga to present
833 was $4.4 \cdot 10^{21}$ g and within the range of estimates of total sulfur release on Mars: $2.2 \cdot 10^{22}$ g
834 (McLennan, 2012), $5.4 \cdot 10^{21}$ g (Gaillard and Scaillet, 2009), $1.7 \cdot 10^{20}$ g (Craddock and Greeley,
835 2009) and $4.5 \cdot 10^{19}$ g (Righter et al., 2009). Dashed line shows a boundary between early and late
836 Hesperian.